euspen's 24th International Conference & Exhibition, Dublin, IE, June 2024
www.euspen.eu

Exploring a compact piezo-driven inchworm motor for LISA space mission

Narendra Mahavar[1,2], Shashwat Kushwaha[1,2], Jonathan Menu[3], Michael Houben[4], Dominiek Reynaerts[1,2]

[1]Department of Mechanical Engineering, KU Leuven, Celestijnenlaan 300, Leuven 3001, Belgium
[2]Member Flanders Make, Belgium
[3]Department of Physics and Astronomy, KU Leuven, Celestijnenlaan 200D, Leuven 3001, Belgium
[4]Founder MACH 8, Belgium

narndra.mahavar@kuleuven.be

Abstract

LISA is an ongoing joint-European effort to develop a system capable of detecting low-frequency gravitational waves in space with high precision. This interferometry-based measurement system suffers from tilt-to-length coupling noise leading to misalignment of laser beam with the detector. An optical beam alignment mechanism actuated with a rotary mechanism will be developed and integrated with the optical bench of the measurement system. This paper talks about the design and development of compact piezo-driven inchworm rotary mechanism adhering to LISA requirements. The device can rotate a shaft by 47 mDeg in a single actuation cycle while maintaining the parasitic translational and angular displacements within ± 0.75 µm and 5.1 mDeg, respectively.

LISA, BAM, Piezo-driven inchworm motor.

1. Introduction

The Laser Interferometer Space Antenna (LISA) [1] is an on-going European effort for a mission to be launched in space in 2035. LISA aims to detect gravitational waves in space with high accuracy and precision. Three spacecraft will therefore be launched in space. These spacecrafts will be arranged in an equilateral triangle form where each arm length is about 2.5 million kilometers. Each spacecraft carries two optical benches which house optical components to detect and measure interference between different pairwise combinations of laser beams, both incoming beams (from the other two spacecraft) and local beams (from the spacecraft itself). Since the system works on the interferometric principle, it suffers from tilt-to-length (TTL) coupling noise. Any kind of parasitic movement of the beam shifts the beam on the detector, leading to TTL noise. One way to address the TTL noise is to laterally shift the incoming and/or local beam to realign with the detector. To achieve this functionality, Beam Alignment Mechanisms (BAM) will be developed and integrated on each optical bench.

A tilted optical flat can shift a beam laterally. Furthermore, the combination of two of these tilted flats enables an arbitrary lateral shift of the beam within a full circle if they are rotated about the axis of the impending beam. To achieve this functionality in space, a space-qualified precision motor with micro-radian rotation resolution is required. Some of the important functional and material requirements for LISA-BAM are shown in Table-1.

Table 1 LISA-BAM functional and material requirements for pre-development

Materials	Avoid ferromagnetic material and optical sources
Cleanliness	Avoid particle generation
Speed	≥ 0.1 °/s
Parasitic transl. disp.	< ±1 µm
Parasitic angular disp.	< 10 mDeg

Non-magnetic piezo-driven precision motors can be divided into three categories based on their working principle namely ultrasonic or resonance motors, inertia driven motors, and inchworm motors. Ultrasonic and stick-slip principle-based motors beat inchworm motors in terms of speed but they generate particles [2]. On the other hand, inchworm principle-based motors produce minimal particles but are relatively slow. Since the desired speed for LISA-BAM mechanism is quite low, inchworm-based motors are preferred if they can provide rotation speed of $0.1\,°/s$. Apart from BAM, article [3] summarizes the development of other extremely stable piezo-driven mechanisms in the scope of LISA, namely, Point Angle Ahead Mechanism (PAAM), Fiber Switching Unit Actuator (FSUA), and In Field Pointing Mechanism (IFPM).

After an initial trade-off of available piezo-driven inchworm motors, a particular inchworm design [4] was chosen for further development due to its lower volume and fewer piezo actuators. As mentioned in Table-1, parasitic translational and angular displacements are some of the important requirements for the motor to maintain the beam stability. Since this data was not available in [4], a prototype was developed using aluminium for quick results. This article presents incremental development of the BAM and reports the findings.

2. Piezo-driven inchworm motor based on C-clamp: BAM-1

2.1. BAM-1 Design

The mechanism uses two identical clamping structures operating in two parallel planes, mounted on a common carrier, but as they are separated by a small gap (Fig. 1 (b)), it allows them to move independently. The rotor is held by the concentric annular clamps (referred to as C-clamps hereafter). Furthermore, the top section also includes a rotation mechanism.

For this inchworm design, a single cycle of rotation refers to the small incremental rotation ($\Delta\theta$) achieved by the shaft after six steps (Fig. 1 (c)) of actuation, which are described below. By sequentially repeating these six steps, large rotation angles can

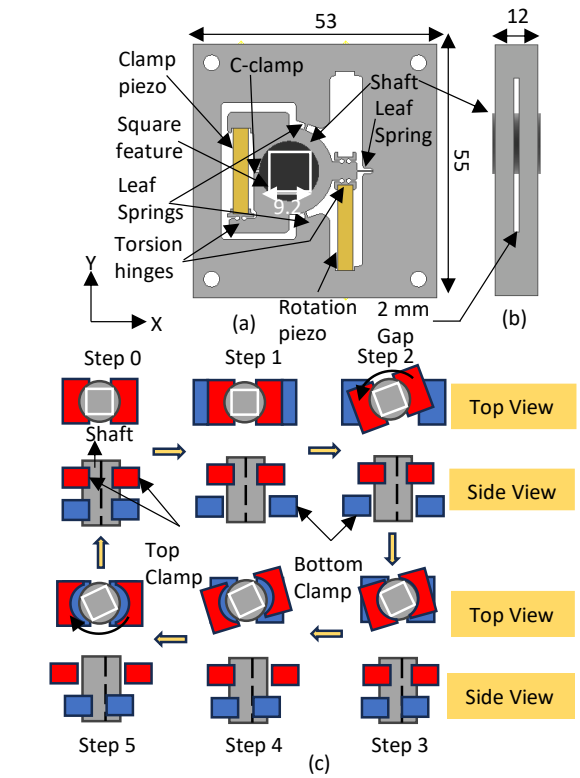

Figure 1. Schematic showing BAM-1 (a) Top view (b) side view, and (c) steps of actuation for single cycle of rotation (all dimensions are in mm).

be achieved. At rest, the shaft is held by both—top and bottom—clamping units.

Step-1: Bottom clamp releases the shaft.

Step-2: Rotation piezo is actuated to rotate the shaft by $\Delta\theta$.

Step-3: Bottom clamp holds the shaft.

Step-4: Top clamp releases the shaft.

Step-5: Rotation piezo comes back.

Step-0: Top clamp holds the shaft.

Note that a 33 mDeg/cycle of rotation was set as a derived requirement assuming that the BAM can perform at least 3 cycles of rotation in a second if actuated at a higher frequency.

2.2. BAM-1 Simulation

Before manufacturing, finite-element static structural simulations were performed to predict the functional operation of design. The indicated holes in Fig. 2 (a) were fixed. The maximum stress developed at the fixed end of L3 leaf spring is 106 MPa at the end of rotation operation which is less than the yield strength of aluminum (~ 240 MPa). Fig. 2 (a) and (b) show the total displacements after clamp opening and rotation operation, respectively.

To open the clamp, opposing equal forces of magnitude 2.3 N were applied at the faces 'Q1' and 'Q2' along the Y-axis to increase the gap between the two by 10 µm . This results into release of the shaft as, 'U1' and 'U2' move away by 1.2 µm along the Y-axis.

For rotation, opposing equal forces of magnitude 57 N were applied at the faces 'Q3' and 'Q4' along the Y-axis to increase the gap between the two by 10 µm. This resulted in a rotation of 28.62 mDeg of the point 'C1' about the center 'C'. Furthermore, the center displaces by about 0.14 µm -0.29 µm about the X-axis and Y-axis, respectively.

2.3. BAM-1 Experimental setup and manufacturing

Tokin piezo elements (AE0505D16DF) were used for this prototype. The size of these piezo elements was 5x5x20 mm^3. Power amplifiers (790A01, AVL) were used to actuate the piezo while actuation waveforms were generated using NI data

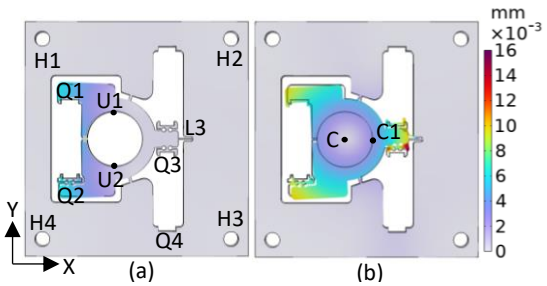

Figure 2. (a) and (b) shows total displacement after clamp opening and rotation, respectively.

acquisition system (PXI 7851R, National Instruments). An optical coordinate measurement machine (Werth VideoCheck HA CMM) was used to measure the position of the shaft from the top. To simplify the measurement process, a square (size of 9.2 mm) was machined at the top of the shaft (Fig. 1 (a)).

BAM-1 prototype was manufactured by wire-EDM. A stainless-steel shaft of 13 mm diameter was used as the rotor of the motor.

2.4. BAM-1 Experiments and results

Two major experiments were performed to characterize the performance of BAM-1. First, the parasitic motion of the shaft was measured during the handover (refer Fig. 3 (a)) of the shaft between the two clamping units. Second, multiple rotation cycles were performed to measure the repeatability of the rotation and the functionality for large angle rotations.

Shaft's center displacement

After each step of handover, the coordinates of the center of the shaft is shown in Fig. 3 (b) for five cycles. The random trajectory of displacements suggests low repeatability of the system. The center of the shaft was found to be displaced by ±15 µm.

Shaft's top plane tilt about the Z-axis

The change in the angle between the unit normal vector of shaft's top plane and the Z-axis (refer Fig. 1 (a)) w. r. t. initial angle at rest after each step of handover is plotted in Fig. 3 (c). The worst-case angle was measured to be 14 mDeg while the BAM requirements for the parasitic angular movement is 10 mDeg.

Multiple rotation cycles of BAM-2

The BAM-2 prototype was programmed to rotate the shaft in an incremental manner. The position of the four points of the square at the top surface of the shaft were measured after 100, 200, 300 and 500 cycles. Fig. 3 (d) shows the angles of rotation of these points calculated about the original center of the shaft's top plane at rest. The average speed of rotation was found to be 10 mDeg/cycle, while the derived LISA-BAM requirement is 33 mDeg/cycle.

Please note that for this inchworm motor design, the center of rotation does not coincide with the center of the C-clamp. This leads to unequal displacement (hence, rotation) of the four corners, as evident from significant drift in the plot. Furthermore, after each cycle of rotation, there are residual displacements in the center of the shaft. This problem can be fixed by constraining the shaft within a bearing.

2.5. BAM-1 Conclusions

From the above results, one can see that BAM-1 does not satisfy desired speed of rotation and parasitic displacements. Furthermore, the shortcomings of this design, as observed during the experiments, are:

- Unknown and multi-point contacts of C-clamp with the shaft ⇒ Large displacements of the rotation center.
- The pre-stressing of the clamping piezo also leads to opening of the C-clamp. This may lead to the unequal

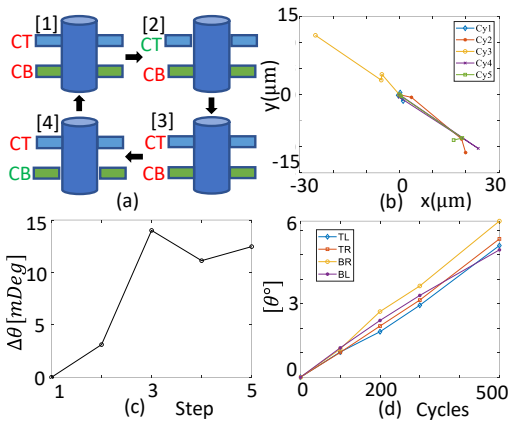

Figure 3. (a) Schematic showing steps during shaft's handover between the two clamps. (Text in red: clamped, green: unclamped), (b) Plot showing shaft's center displacement after each step of handover for five cycles, (c) Plot showing the tilt of the shaft: change in the angle between the unit normal vector of shaft's top plane and the Z-axis w. r. t. initial angle at rest, (d) Plot showing angle of rotation of the four points of the square at the top surface of the shaft, measured after 100, 200, 300 and 500 number of cycles. (TL: top left, TR: top right, BR: bottom right, BL: bottom left coordinates of the square at the top of the shaft).

diameter of the C-clamps of the two clamping sections, resulting in initial tilt of the shaft about the Z-axis.

3. Piezo-driven inchworm motor based on three-point contact: BAM-2

3.1. BAM-2 Design

To overcome the above-mentioned shortcomings, a new design called 'Cymbal design' or 'BAM-2' (Fig. 4 (a)) is proposed. This design has two main advantages over BAM-1.

- The clamping mechanism has deterministic three-point contact with the shaft. This will reduce the parasitic angular and translational displacements of the shaft.
- Secondly, additional elastic hinges have been added to decouple the pre-stress on the piezo from the clamp opening. The stiffness of these hinges (refer Fig. 4 (a)) is designed to be an order of magnitude less than the stiffness of the clamp. During piezo pre-stress, only the hinges undergo bending without deforming the cymbal clamping.

3.2. BAM-2 Simulation

For simulation, the indicated holes in Fig. 5 (a) were fixed. The maximum stresses developed at the fixed end of L3 leaf spring and at the center of the cymbal beam are 90 MPa and 120 MPa, respectively which are less than the yield strength of aluminum. Fig. 5 (a) and (b) shows the total displacements after clamp opening and rotation operation, respectively.

To open the clamp, equal forces of magnitude 49 N were applied at the faces 'Q1' and 'Q2' along the Y-axis to increase the gap between the two by 10 μm. This results into a total increment in the distance between point 'A' and 'B' by 3 μm.

For rotation, opposing forces of magnitude 18 N were applied at the faces 'Q3' and 'Q4' along the Y-axis to achieve a rotation of 45.13 mDeg of the point 'C1' about the center 'C'

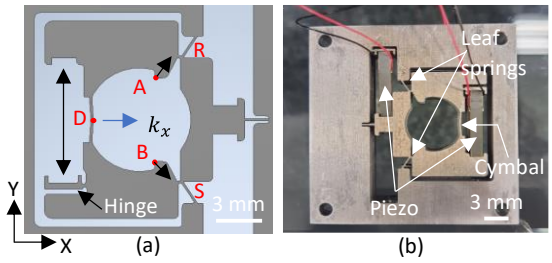

Figure 4. BAM-2 (a) CAD design (b) Image of the fabricated part.

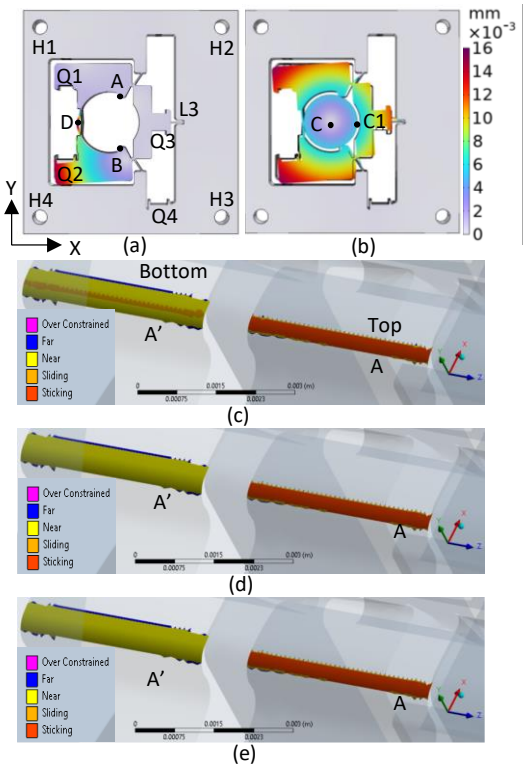

Figure 5. (a) and (b) shows total displacement after clamp opening and rotation, respectively. Contact status at point 'A' when (c) clamped from top and bottom and at the end of (d) bottom clamp open, and (e) subsequent rotation at the top.

which is assumed to remain fixed. Furthermore, the center displaces by about 0.16 μm and -0.05 μm. about the X-axis and Y-axis, respectively.

Additional simulations were performed to understand the contact status and the contact reaction forces. The contacts between the shaft and the contact points 'A', 'B' and 'D' were defined as frictionless and bonded (no relative motion at the contact location) for the bottom and top section respectively.

A three-step finite-element static structural simulations (Ansys, 2023) was performed. Step-1: to simulate the shaft clamping, equal and opposing forces of 62.2 N are applied at Q1 and Q2 faces (refer Fig. 5 (a)) to bring them closer. This results in a certain amount of force on the shaft which is balanced by the reaction forces at 'A' and 'B'. In step-2 bottom clamp is opened by 10 μm to release the shaft from the bottom while it is still held from the top clamp. In step-3 the top section is rotated by 45 mDeg about the center 'C'. Fig. 5 (d) and (e) show the plots of contact status at points 'A' (top section) and 'A'' (bottom section) at the end of the opening of the bottom clamp, and after subsequent rotation at the top, respectively.

For the bottom section, initially, the shaft is held by 5.94 N clamping reaction force from line contact at 'A''. After the bottom clamp opening, the contact reaction force at point 'A'' reduces to 2.55 μN as it moves away from the shaft by 1.8 μm. The plots also confirm this behavior where the line contact (sliding contact shown in brown color) in Fig. 5 (c) vanishes completely (Fig. 5 (d)). It further reduces to 2.52 μN after the subsequent rotation from the top clamp. Fig 5 (e) shows that there is no sliding at the bottom while the top section undergo rotation, ensuring no particle generation.

For the top section, initially, the shaft is held by 7.52 N clamping reaction force from line contact at 'A'. After the bottom clamp opening, the contact reaction force at point 'A' reduces to 6.11 N, but later increases to 7.64 N due to additional force resulting from the subsequent rotation from the top clamp. These results show that when the top section undergoes

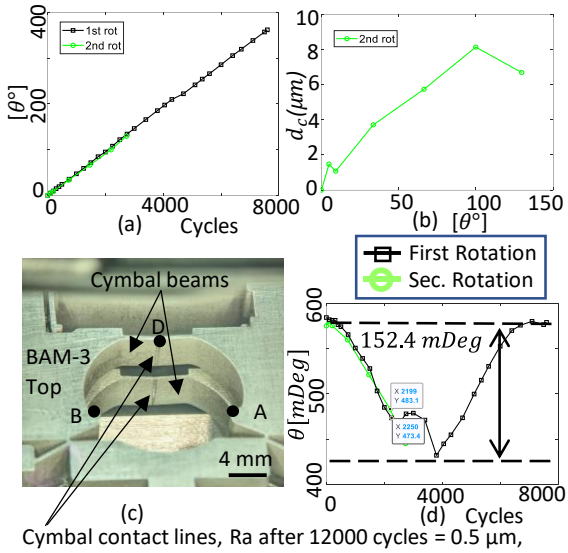

Cymbal contact lines, Ra after 12000 cycles = 0.5 µm, as opposed to 1.6 µm at the beginning

Figure 6. (a) The angle of rotation of the shaft in function of cycles, (b) Shaft's center displacement with respect to the angle of rotation, (c) Image of the actuator module cymbals showing contact lines after 12000 cycles of rotation, (d) The angle between unit normal vector of the shaft's top plane and the Z-axis with respect to the cycles.

rotation, there is minimal friction/contact between the shaft and the bottom contact points.

3.3 BAM-2 Experiments and results

As described earlier for BAM-1, the same manufacturing technique, material, power amplifier, data acquisition system, measurement system and shaft were used for BAM-2. An image of the fabricated BAM-2 is shown in Fig. 4 (b). The part was fabricated within 6 µm from the nominal dimension (diameter of the circle defined by points 'A', 'B', and 'D'). Space-qualified multi-stack piezo actuators from PI were used in this prototype. The size of the piezo (PICMA, P-883.51) was 3x3x18 mm³. The position of the shaft was measured for a first rotation of 362° by performing 7600 stepping cycles, and for a second rotation of 129° performing 3000 stepping cycles. The BAM-2 prototype had already done 1300 run-in cycles before these measurements. From the recorded data, the angle of rotation, shaft's center displacement and the tilt of the shaft about the Z-axis were extracted.

Angle of rotation

Fig. 6 (a) shows the angle of rotation of the shaft for a range of 362° with respect to the number of cycles. The average rate of rotation was found to be **(47.61 ± 0.25) mDeg/cycle** when the rotation piezo was actuated at 90 V generating 11 µm. displacement. The speed can be increased up to 80.5 mDeg/cycle by driving it at the maximum rated voltage of 120 V. As per the requirement, the desired speed of 0.1 °/s can be achieved successfully.

Shaft's center displacement

As per requirement, the parasitic displacements should be within a circle of radius 1 µm. After 129° of rotation, no further rotation was observed for the shaft. This is due to wear of the contact surface after roughly 12000 cycles. The contact lines have become smoother (refer Fig. 6 (c)) resulting in reduced friction. Fig. 18 shows the center displacement of the shaft during second rotation for 129° of rotation. The center displaces by ±**4 µm**.

Shaft's top plane tilt about the Z-axis

Fig. 6 (d) shows the plot of the angle between unit normal vector of the shaft's top plane and the Z-axis with respect to the number of cycles. At the beginning, the shaft's top plane is not normal to the XY-plane, resulting in an initial tilt of about 0.58 Deg. During the rotation, a maximum deviation of this tilt was found to be around **152.4 mDeg**, which goes back to the initial tilt after full rotation. During the second rotation, a **10 mDeg** repeatability of this tilt angle was measured as compared to the first rotation. The behavior remains thus similar to the first full rotation.

3.4 BAM-2 Conclusion

The BAM-2 mechanism works as intended and is capable of full rotation at the desired speed. But this design is off by 4 and 15 times for the parasitic translational and angular BAM requirements, respectively. Further, material selection/surface treatment is important for a satisfactory performance of the BAM in long-run.

4. Discussion and conclusion

Table 2 Comparison of BAM-1 and BAM-2 performance till 6° of rotation.

BAM	Avg. Speed	Para. ang. disp.	Para. transl. disp.
BAM-1	10 mDeg/Cy	14 mDeg	±15 µm
BAM-2	47 mDeg/Cy	5.1 mDeg	±0.75 µm

Since BAM-1's measurements were only performed till 6° of rotation, Table-2 provides the performance comparison between the two designs till 6° of rotation. As shown BAM-1's parasitic displacements are worse than BAM-2's. This is due to the low positional repeatability of the C-clamp based BAM-1 compared to BAM-2. Furthermore, BAM-2 results are far better than BAM-1 in terms of speed, and repeatability. In a longer test, BAM-2 shows degradation in holding of shaft due to wear. The wear of contact points is a clear culprit.

Recommendation: It is clear that the designs explored here are incompatible with the parasitic displacement requirements for LISA-BAM. One of the ways to address these issues is to hard constrain the shaft translation and tilt, while allowing free rotation. For this reason, it is proposed to include a bearing in the design and develop a new prototype. The design of the 3-point contact of the BAM-2 can be adapted to be used with bearings.

Material selection and use of coatings to reduce the wear and improve the life of the mechanism is another open issue. The tribological study of the BAM is required.

Acknowledgement

The authors thank the Belgian Federal Science Policy Office (BELSPO) for the provision of financial support in the framework of the PRODEX Programme of the European Space Agency (ESA) under contract number PEA 4000131558.

References

[1] K. Danzmann, "LISA Mission Overview", *Advances in Space Research* Vol. **25**, Issue 6, 2000, 1129 – 1136.

[2] K. Spanner, and B. Koc, (2016, February). Piezoelectric motors, an overview. In *Actuators* (Vol. **5**, No. 1, p. 6). MDPI.

[3] J. Pijnenburg, N. Rijnveld, and H. Hogenhuis (2012, September). Extremely stable piezo mechanisms for the new gravitational wave observatory. In *Modern Technologies in Space-and Ground-based Telescopes and Instrumentation II* (Vol. **8450**, pp. 105-119). SPIE.

[4] S. Shao, S. Song, K. Liu, and M. Xu, (2019). A piezo-driven rotary inchworm actuator featured with simple structure and high output torque. *International Journal of Applied Electromagnetics and Mechanics*, **59(1)**, 317-325.